JOURNAL OF VIROLOGY, Feb. 2006, p. 1280–1289 Vol. 80, No. 3
0022-538X/06/$08.00+0 doi:10.1128/JVI.80.3.1280–1289.2006

Palmitoylations on Murine Coronavirus Spike Proteins Are Essential for Virion Assembly and Infectivity

Edward B. Thorp,† Joseph A. Boscarino, Hillary L. Logan, Jeffrey T. Goletz, and Thomas M. Gallagher*

Department of Microbiology and Immunology, Loyola University Medical Center, Maywood, Illinois 60153

Received 22 June 2005/Accepted 11 November 2005

Coronavirus spike (S) proteins are palmitoylated at several cysteine residues clustered near their transmembrane-spanning domains. This is achieved by cellular palmitoyl acyltransferases (PATs), which can modify newly synthesized S proteins before they are assembled into virion envelopes at the intermediate compartment of the exocytic pathway. To address the importance of these fatty acylations to coronavirus infection, we exposed infected cells to 2-bromopalmitate (2-BP), a specific PAT inhibitor. 2-BP profoundly reduced the specific infectivities of murine coronaviruses at very low, nontoxic doses that were inert to alphavirus and rhabdovirus infections. 2-BP effected only two- to fivefold reductions in S palmitoylation, yet this correlated with reduced S complexing with virion membrane (M) proteins and consequent exclusion of S from virions. At defined 2-BP doses, underpalmitoylated S proteins instead trafficked to infected cell surfaces and elicited cell-cell membrane fusions, suggesting that the acyl chain adducts are more critical to virion assembly than to S-induced syncytial developments. These studies involving pharmacologic inhibition of S protein palmitoylation were complemented with molecular genetic analyses in which cysteine acylation substrates were mutated. Notably, some mutations (C1347F and C1348S) did not interfere with S incorporation into virions, indicating that only a subset of the cysteine-rich region provides the essential S-assembly functions. However, the C1347F/C1348S mutant viruses exhibited relatively low specific infectivities, similar to virions secreted from 2-BP-treated cultures. Our collective results indicate that the palmitate adducts on coronavirus S proteins are necessary in assembly and also in positioning the assembled envelope proteins for maximal infectivity.

Palmitoylation is a common posttranslational modification that can influence protein trafficking and protein-protein and protein-membrane interactions. The hydrophobic acyl chains are linked in thioesterification reactions to cysteine residues residing in the cytoplasmic tails of several viral membrane glycoproteins, including the influenza virus hemagglutinin, paramyxovirus F, vesicular stomatitis virus (VSV) G, Sindbis virus (SV) E1, retrovirus Env, baculovirus gp64, and coronavirus spike (S). The importance of these lipid modifications to viral glycoprotein structure is not precisely known; however, it is reasonable to assume that they act to position cytoplasmic tails at juxtamembrane locations, thereby contributing a membrane anchoring that is secondary to protein transmembrane spans. This tethering to the cytoplasmic leaflets of lipid bilayers may have several distinct functional ramifications. There is evidence that palmitate adducts alter protein transport in the cellular exocytic pathway (34), assist in clustering glycoproteins into lipid microdomains (5, 55), and enforce membrane anchoring during the refolding events accompanying viral glycoprotein-mediated membrane fusions (50). Given these varied modes by which the acyl groups can affect membrane proteins, it is perhaps not surprising that each virus has a unique dependence on these modifications. For example, Sindbis (39), VSV (53), and influenza virus H3 (18) infections are not compromised by substitution of their palmitoylated cysteines, while influenza virus H1 (56) and human immunodeficiency virus infections (35) clearly are.

This report focuses on the infection requirements for palmitoylation of coronavirus proteins. The coronaviruses are enveloped plus-strand RNA viruses responsible for severe respiratory and gastrointestinal diseases in humans, domesticated livestock, and birds (29). They are characterized by their remarkably large (~600-kDa) trimeric S glycoprotein projections, about 500 of which protrude uniformly from each virion envelope (9). The S proteins function during virus entry as receptor-binding ligands and also as mediators of virus-cell membrane fusion (6). Some S proteins, notably those encoded by the murine hepatitis viruses (MHVs), are cleaved by *trans*-Golgi furin-like proteases into two similarly sized ~90-kDa fragments, termed S1 and S2 (10). The carboxy-terminal S2 fragments are embedded into virion and infected-cell membranes, and at the boundaries between transmembrane spans and cytoplasmic tails, those from all serogroups have a region containing 7 to 10 cysteine residues within an 18- to 22-amino-acid stretch (see Fig. 9A). More than one of these cysteines are modified by palmitoylation (2), but the exact acylated residues are not yet known for any coronavirus.

The conservation of this remarkably dense cluster of cysteines clearly suggests an important functional relevance. In beginning this study, we hypothesized that palmitates in this region were crucial for virus assembly. Coronaviruses assemble intracellularly, with complete particles budding into the lumen of the endoplasmic reticulum (ER) and *cis*-Golgi apparatus

* Corresponding author. Mailing address: Department of Microbiology and Immunology, Loyola University Medical Center, 2160 South First Avenue, Maywood, IL 60153. Phone: (708) 216-4850. Fax: (708) 216-9574. E-mail: tgallag@lumc.edu.

† Present address: Department of Medicine, Columbia University, New York, NY 10032.

(45) and then transporting out through the exocytic pathway. Given that secreted, virion-associated S proteins are known to be acylated (41) and given that transport-incompetent S proteins produced in the presence of tunicamycin are palmitoylated (46), one can infer that the cysteine modifications take place shortly after S synthesis in the ER, before the S cytoplasmic tails are buried in the interior of assembled virions and thus occluded from the palmitoyl acyltransferases (PATs) responsible for attaching the lipid adducts (40, 48). We considered the possibility that the dense cysteine clusters evolved in response to the need for rapid S palmitoylation at or near the ER, before anterograde transport to the nearby virus assembly site. Indeed, PAT activities may be at a relatively low level in the ER (12, 24), and this paucity of enzyme could be a selective force for the expansion of cysteine substrates.

A clear inference from this point of view is that S-protein palmitoylation is a prerequisite for the production of infective coronaviruses. This hypothesis has not been tested. To date, the functional importance of the cysteine-rich region has been addressed outside of the context of natural coronavirus infections. Using S cDNAs derived from the prototype MHVs, this cysteine-rich region was targeted for mutagenesis, and spike cDNAs were expressed with vaccinia vectors (2, 7). Findings indicated that two or more cysteines are indeed sites for acylation and that replacement of certain cysteines with serine reduces but does not eliminate receptor-dependent, pH-independent spike protein cell-cell membrane fusion activities (2). More recently, the cysteine-rich region was shown to be essential for virion assembly (3, 54), making it clear that, at least for the murine coronaviruses, this portion of the S protein has a role in two distinct stages of the virus growth cycle.

In this study, we addressed the functional importance of posttranslational S acylations using both pharmacologic and molecular genetic approaches. With 2-bromopalmitate, a specific inhibitor of protein palmitoylation (51), we traced a crucial importance of palmitates for creating infective virions. This pharmacologic strategy complements molecular genetic analyses, eliminating caveats associated with genetic approaches caused by unanticipated influences of substituted or deleted amino acids. Since there are widely used, facile reverse genetics systems for studying coronaviruses (23), we also introduced selected cysteine substitutions into recombinant MHVs. Our collective findings point to an essential role for acylations in creating the virion membrane protein interactions required for particle infectivity. The posttranslationally added lipids influence protein-protein interactions and suggest a novel requirement for palmitates in coronavirus virions.

MATERIALS AND METHODS

Cells and viruses. All cell lines were propagated as adherent monolayer cultures. Murine 17cl1 fibroblasts (42) were grown in Dulbecco's modified Eagle medium (DMEM) containing 5% tryptose phosphate broth (Difco Laboratories) and 5% heat-inactivated fetal bovine serum (ΔFBS). HeLa-tTA (tTA denotes tetracycline-controlled transactivator) (15), RK13, FCWF, and BHK cells were grown in DMEM supplemented with 10% ΔFBS (Atlas Biologicals, Fort Collins, CO). HeLa-tTA-CEACAM (*c*arcino *e*mbryonic *a*ntigen *c*ell *a*dhesion *m*olecule, isoform 1a, cell line no. 3 [32]) was cultured in DMEM–10% ΔFBS containing 2.5 μg/ml mycophenolic acid, 250 μg/ml xanthine, 20 μg/ml hypoxanthine, and 100 μg/ml G418. Soluble-receptor secreting 293 EBNA-N-CEACAM$_{Fc}$ (sMHVR$_{Fc}$) cells (14) were grown in DMEM–10% ΔFBS containing the antibiotics G418 (100 μg/ml) and hygromycin B (200 μg/ml). All growth media were buffered with 0.01 M sodium HEPES (pH 7.4).

Coronavirus strains JHM (prototype strain MHV-4) (52), JHM-X (22), and A59 (36) were plaque purified three times on HeLa-CEACAM cells and subsequently propagated after a 1-h adsorption on 17cl1 cells at a low multiplicity of infection (0.01 PFU/cell) in serum-free medium with 0.01% (wt/vol) bovine serum albumin. Inoculums were replaced with growth medium containing 2% ΔFBS and cell supernatant harvested at 18 h postinfection (hpi), followed by clarification of medium by differential centrifugation to remove cellular debris (sequential spins of 15 min at 2,000 × *g* followed by 30 min at 10,000 × *g*). Infectivities were determined by plaque assay, using either HeLa-CEACAM or 17cl1 as indicator cells in DMEM–1% ΔFBS and 0.5% (wt/vol) Noble agar (Difco). Vaccinia virus recombinants vTF7.3 (13) and vTM1-S-JHMX (20), encoding S of strain JHMX, were generated and propagated in RK13 cells as described previously (20). VSV and SV were propagated in BHK cells after a low multiplicity of infection and collected from cells after the first signs of cytopathic effect. VSV and SV were clarified as described above for MHV by differential centrifugation prior to application onto cell monolayers.

Recombinant viruses. Targeted RNA recombination (21) was used to create site-directed mutant MHV recombinants. To maximize the potential recognition of site-directed mutants with impaired membrane fusion functions, we used plasmids and parental recombinant MHVs derived from the highly syncytial JHM strain (27). Briefly, plasmid pGssS4 (30), encoding the S protein from MHV JHM (denoted in reference 26 as the "SD" or San Diego JHM strain), was mutated at codon 310 to create G310S. The G310S mutation stabilizes S1-S2 connections, thereby retaining complete S1-S2 complexes during virion purification procedures (26). Mutagenic primers encoding portions of the cysteine-rich region were then used in a series of PCRs to create fragments with missense changes at S codons 1344 (C to S), 1347 (C to S), and 1348 (C to F). A silent BstBI site was also engineered in the PCR products at codon positions 1349 to 1350 to simplify subsequent mutagenesis of the cysteine-rich region. A series of mutant S cDNAs was then excised from the pGssS4 plasmids with AvrII and SbfI and used to replace the corresponding regions in pJHM.CA (26), yielding the separate plasmids pJHM-G310S, pJHM-G310S/C1348F, pJHM-G310S/C1347S/C1348F, and pJHM-G310S/C1344S/C1347S/C1348F. These plasmid DNAs were linearized by digestion with PacI and used as templates for in vitro transcription reactions, using T7 RNA polymerase and mMessage mMachine reagents (Ambion, Inc., Austin, TX). In vitro transcripts representing the 3′ 9,336 nucleotides of the MHV genome (~10 μg of each mutant transcript) were electroporated into ~10^7 feline FCWF cells that were infected 6 h earlier with recombinant coronavirus feline MHV-JHM (21, 27), using a Bio-Rad Gene Pulser II. The electroporated FCWF cells (~10^5) were then added to T25 flasks seeded with ~10^6 murine 17cl1 cells. Recombinant JHM viruses were identified by the development of syncytia in the 17cl1 monolayers and then isolated by three cycles of plaque purification on 17cl1 cells. All site-directed mutations were confirmed in the recombinant viruses by isolating RNAs from infected cells and performing reverse transcription-PCR and sequencing of the relevant cDNA fragments.

Infections and metabolic labeling. Infections were carried out on monolayer cultures, typically ~10^5 17cl1 cells per cm^2. At various times postinfection, media were removed and cells rinsed extensively with isotonic saline. For radiolabeling with ^{35}S amino acids, cells were first incubated for 30 min at 37°C in labeling medium (methionine- and cysteine-free DMEM containing 1% dialyzed ΔFBS) and then replenished with fresh labeling medium containing 50 to 100 μCi per ml ^{35}S translabel (MP Biomedical, Irvine, CA) and incubated for 2 to 8 h at 37°C. Media were then collected and cells dissolved in NP-40 buffer (25 mM HEPES [pH 7.4], 100 mM NaCl containing 0.5% NP-40, and 0.1% protease inhibitor [Sigma P2714]), to 10^6 cell equivalents per ml lysate. In some experiments, cells were dissolved in NP-40/DOC buffer (25 mM HEPES [pH 7.4], 100 mM NaCl containing 0.5% NP-40, 0.5% sodium deoxycholate, and 0.1% protease inhibitor) to preserve S-M interactions (28). To detect posttranslational palmitoylations, cells were incubated in complete medium containing 50 μCi per ml [^{3}H]palmitate (MP Biomedical) for 6 h at 37°C and then rinsed extensively with saline and dissolved in NP-40 buffer.

Virus purification. Media collected from infected cultures were chilled and kept at 4°C throughout purification. Media were centrifuged for 10 min at 2,000 × *g*, then for 10 min at 20,000 × *g*, and then overlaid onto 30% and 50% (wt/wt) sucrose cushions, each in HNB buffer (50 mM HEPES [pH 7.4], 100 mM NaCl, 0.01% bovine serum albumin). Virions were equilibrated at the 30%-50% sucrose interfaces, typically using a Beckman Spinco SW28 rotor at 28,000 rpm for 4 h, and recovered by fractionation from air-gradient interfaces. In some experiments, virus-containing fractions were diluted with HNB, subjected to an additional round of purification on fresh sucrose gradients, and then concentrated by pelleting through 30% sucrose cushions. Purified virions were resuspended in HN buffer (50 mM HEPES [pH 7.4], 100 mM NaCl) and stored at 4°C in silanized glass vials.

Immunoprecipitations and immunoblotting. S proteins and S-M complexes were captured onto protein A magnetic beads (NEB Corporation, Inc.) conjugated with N-CEACAM-Fc (no. 56) (14). Briefly, nuclei were first removed from cell lysates by centrifugation at 2,000 × *g* for 5 min. One-milliliter volumes were then mixed with 0.2 ml of 5 μg per ml N-CEACAM-Fc and 0.01 ml of magnetic beads for 2 h at 22°C. Beads were collected magnetically and rinsed with three sequential 1-ml volumes of NP-40 or NP-40/DOC buffer. Proteins were eluted from beads by adding 0.1 ml of sodium dodecyl sulfate (SDS) sample solubilizer (0.06 M Tris-HCl (pH 6.8), 2% SDS, 5% 2-mercaptoethanol, 2.5% Ficoll, 0.01% bromphenol blue) and heating to 95°C for 5 min. For radioactive samples, SDS-polyacrylamide gel electrophoresis (PAGE) was followed by fluorography. For nonradioactive samples, SDS-PAGE was followed by electrophoretic transfer to polyvinylidene difluoride membranes, which were then blocked with TBS-T-M (25 mM Tris-HCl [pH 7.5], 140 mM NaCl, 27 mM KCl, 0.05% Tween 20 to 5% nonfat milk powder). S proteins were detected with murine monoclonal antibody (MAb) 10G (1:10,000 in TBS-T-M), kindly provided by Fumihiro Taguchi. M proteins were detected with murine MAb J.3.1 (1:5,000 in TBS-T-M), a generous gift from John Fleming. Horseradish peroxidase-conjugated secondary antibodies and Western-Lightning reagents (both from Perkin-Elmer, Inc.) were used for chemiluminescence detection of the bound antibodies.

Detergent-resistant membranes. S glycoproteins were evaluated for partitioning into detergent-resistant membranes (DRMs) using methods described previously (44). Infected 17cl1 or HeLa-CEACAM cells were rinsed with isotonic saline, chilled to 4°C, and dissolved in ice-cold TNE-TX100 (50 mM Tris-HCl [pH 7.4], 100 mM NaCl, 1 mM EDTA, 1% Triton X-100) to 10^7 cells/ml. After 30 min at 4°C, cell extracts were passed five times through a 27-gauge needle and centrifuged (700 × *g* for 5 min) to remove nuclei. Postnuclear supernatants were mixed with equal volumes of 80% (wt/vol) sucrose in TNE–1.0% TX-100 containing 0.1% protease inhibitor (Sigma), were placed in ultracentrifuge tubes, and overlaid sequentially with 7 ml of 38 or 30% (wt/vol) (as indicated) and 2.5 ml of 5% (wt/vol) sucrose in TNE. Following centrifugation at 4°C for 18 h at 285,000 × *g* in a Beckman SW41 rotor, fractions were collected from air-gradient interfaces. Aliquots of each fraction were then mixed with SDS solubilizer (final concentration, 63 mM Tris-HCl [pH 6.8], 2% [wt/vol] sodium dodecyl sulfate, 2.5% [wt/vol] Ficoll, 0.0025% [wt/vol] bromophenol blue, 5% [vol/vol] 2-mercaptoethanol), heated at 95°C for 5 min, and processed by SDS-PAGE and immunoblotting. To assess the solubilization and fractionation of cell membranes during preparation of DRMs, the standards transferrin receptor and ganglioside GM1 were detected in gradient fractions using anti-transferrin receptor antibodies and cholera toxin-peroxidase conjugate, respectively (16). In assays designed to specifically detect only those S proteins on the plasma membrane, cells were exposed to sulfo-NHS-biotin from Pierce Corporation (catalog no. 21335). Cells were suspended in a minimal volume of phosphate-buffered saline (PBS) (pH 8.0), biotinylated (1 mg/ml biotin) at 4°C for 20 min, and further rinsed three times in cold 50 mM Tris-containing buffer at pH 8.0 to quench unreacted biotin. Cells were subsequently rinsed with ice-cold PBS and subjected to TX-100 extraction and fractionation as aforementioned. Biotinylated proteins were captured with streptavidin-Sepharose beads and processed by immunoblotting as described above.

RESULTS

Effect of 2-BP on MHV infectivities. In our initial experiments, we applied 2-bromopalmitate (2-BP), a general inhibitor of protein palmitoylation (51), to murine fibroblast cells that had been inoculated with various enveloped viruses. After overnight incubations, media were then removed for infectivity determinations. We found that 2-BP at doses up to 12 μM had little effect on VSV or Sindbis virus infections (Fig. 1); this was an expected finding given that site-directed mutation of the palmitoylation sites in these viruses does not impair their infectivities (39, 53). In sharp contrast, coronavirus MHV (strain JHMX) infections were potently inhibited, with doses as low as 0.1 μM reducing yields by fivefold and with 1,000- to 10,000-fold-reduced infectivities at the highest, 12-μM doses (Fig. 1). These 2-BP doses effecting significant infectivity reductions were extraordinarily low, being about 100 to 1,000 times lower than those typically used to generally block protein palmitoylations (47) (51).

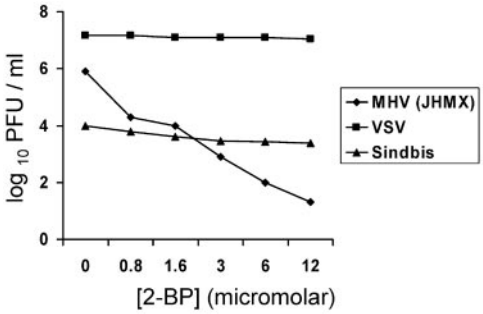

FIG. 1. Effect of 2-BP on virus infectivities. 17cl1 murine fibroblast monolayers (10^5 cells/cm^2) were inoculated with the indicated RNA viruses at 0.1 PFU per cell. At 1 h postinfection, media were aspirated and replaced with fresh growth media containing the indicated concentrations of 2-BP. Fifteen hours later, media were removed, and infectivities were determined by plaque titration using 17cl1 cell monolayers as indicator cells.

To determine whether 2-BP blocked production or secretion of MHV particles, media from ^{35}S-labeled cultures were collected and virions purified on sucrose density gradients. Here we investigated the effect of 2-BP on two prototype MHV infections, with strains JHMX and A59, to determine whether strain-specific drug sensitivities might be evident. For both strains, the 2-BP exposures had little effect on the quantity of ^{35}S virions obtained from culture media, at low doses creating nominal increases in ^{35}S particle yields while reducing the yields about twofold at the higher 5 and 10 μM levels (Fig. 2). Notably, all of the virion preparations had identical 1.18-g/ml buoyant densities (data not shown). Using plaque assays, specific infectivities (PFU/^{35}S cpm) were calculated. For both of the MHV strains, the 2-BP exposures effected very significant and very similar reductions in specific infectivities (Fig. 2). These findings indicated that the 2-BP-treated cultures secreted noninfectious particles and suggested that the palmitate adducts on virion proteins are essential components of infective virions.

These convincing, direct relationships between the 2-BP dose and MHV particle infectivities contrasted with an interesting bimodal effect of 2-BP on MHV-induced syncytial developments. These effects were best observed in cultures infected with strain JHMX, which is powerfully syncytial relative to strain A59. Remarkably, the MHV-induced syncytia were actually promoted by low (0.5 to 1 μM) doses of 2-BP (Fig. 3A to D). Thus, the low-dose 2-BP treatments changed infection transmission patterns, blocking virion-associated transmissions while preserving, and at specific doses even modestly enhancing, the spread of infection via syncytia. This phenomenon was confirmed by performing plaque assays in which overlying growth media were supplemented with 2-BP. Plaques developed in the presence of up to 3 μM 2-BP, but infectious virions could not be recovered from them, indicating syncytial expansion without concomitant secretion of infectious MHV particles. However, the higher 5 to 10 μM doses of 2-BP did block syncytia, to nearly undetectable levels (Fig. 3E and F). Notably, these interesting responses to specific 2-BP doses were not unique to 17cl1 cell cultures, since we observed a parallel pattern of decreasing virion infectivity and increasing syncytia with infected HeLa-CEACAM cells (data not shown).

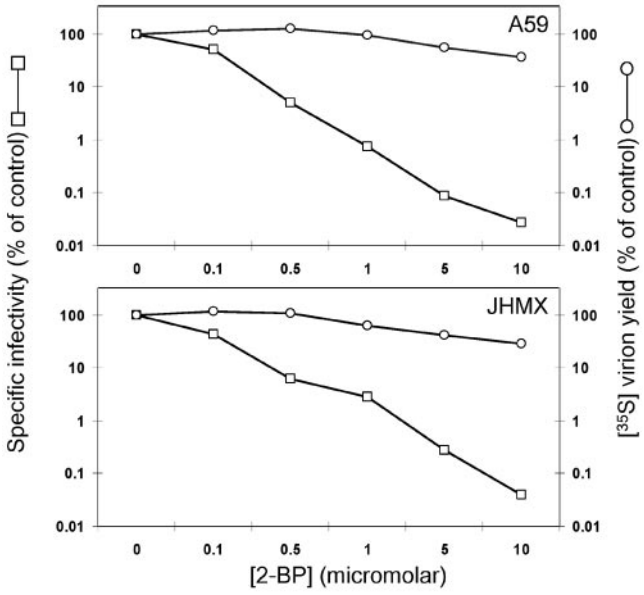

FIG. 2. Effect of 2-BP on MHV-specific infectivities. MHV-infected 17cl1 cells (multiplicity of infection = 2) were incubated from 1 to 16 hpi with the indicated 2-BP doses. Media were then removed and replaced with ^{35}S-labeling media containing the same 2-BP concentrations. Four hours later, media were collected and ^{35}S-labeled virions purified on sucrose density gradients. Banded ^{35}S-labeled virions were quantitated by scintillation spectrometry and radioactive virus yields plotted relative to controls. Specific infectivities of purified virions (PFU/^{35}S cpm) were determined by plaque assay on 17cl1 cells and plotted relative to control values. In the absence of 2-BP, A59- and JHMX-specific infectivities were 2.06 and 1.55 PFU/^{35}S cpm, respectively.

Effect of 2-BP on S protein-M protein interactions. To explain these phenomena, in which particle infectivities declined as syncytia increased, we hypothesized that 2-BP very effectively inhibited ER-localized PAT activities, leaving newly synthesized, uncleaved S proteins underpalmitoylated and unable to participate properly in the virion assembly reactions taking place at the *cis*-Golgi complex (19). Some of these underpalmitoylated S proteins would then remain with infected cells, perhaps advancing through the exocytic pathway to plasma membranes, thus modestly increasing syncytia in a narrow range of 2-BP drug exposure (Fig. 3).

This hypothesis contends that S proteins are depleted in the virions secreted from 2-BP-treated cells, a reasonable possibility given that S proteins are dispensable for MHV particle assembly and secretion (49). Absence of S would not be apparent from the results shown in Fig. 2, because they comprise a very small fraction of the ^{35}S radioactivity in MHV particles. Therefore, we evaluated the effect of 2-BP on S protein secretion by collecting media and dissolving cell monolayers in a series of 2-BP-treated, MHV A59-infected cultures. S proteins were then captured using N-CEACAM-Fc (14) and imaged by Western immunoblotting. As predicted, the immunoblots revealed that 2-BP did not block S-protein synthesis and accumulation but did block secretion into media (Fig. 4). Quantifications obtained by titrating the samples in subsequent immunoblot assays (data not shown) indicated that the cell-associated proportion of S proteins steadily rose with increased 2-BP dose, from ~60% to ~95%, while the proportion of S proteins in media correspondingly declined from ~40% to ~5%. These data were consistent with the hypothesis that underpalmitoylated S proteins are excluded from virions and

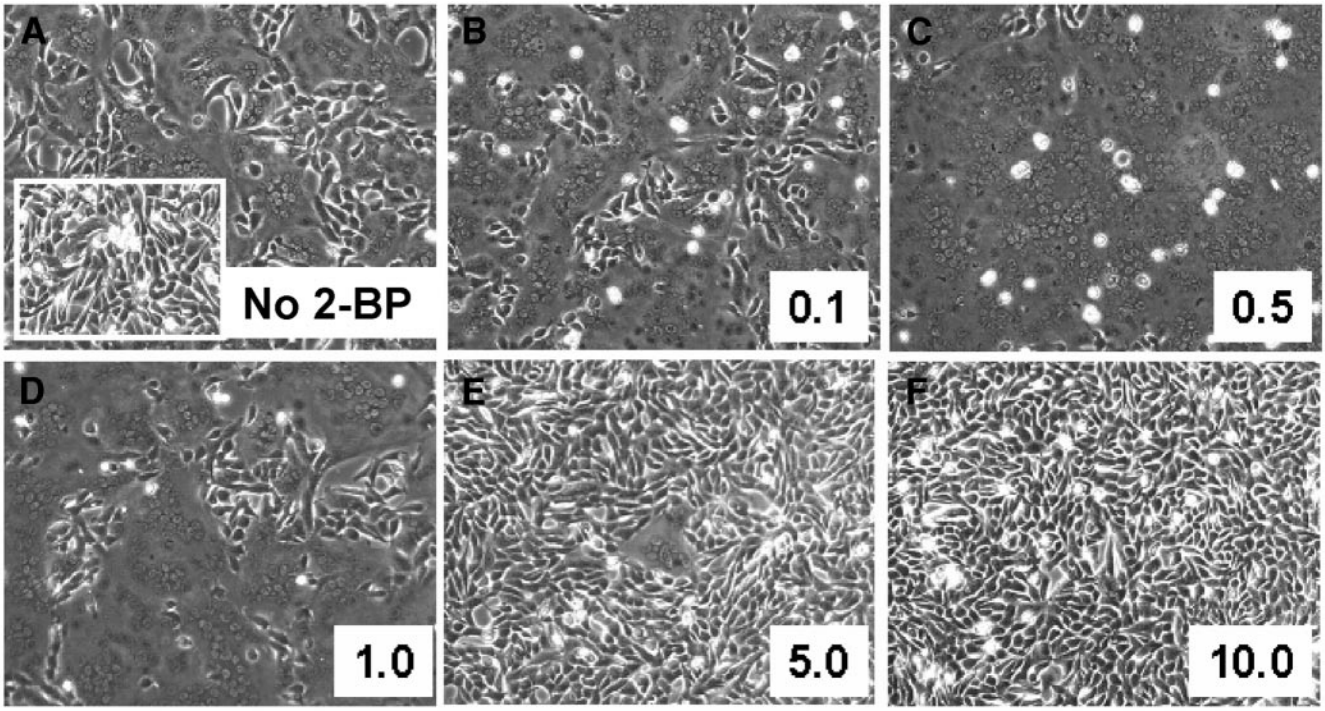

FIG. 3. Effect of 2-BP on MHV-induced syncytia. MHV (strain JHMX)-infected 17c1l cells were incubated from 1 to 16 hpi with the indicated micromolar concentrations of 2-BP and photographed by phase-contrast microscopy. Inset in panel A depicts uninfected cells.

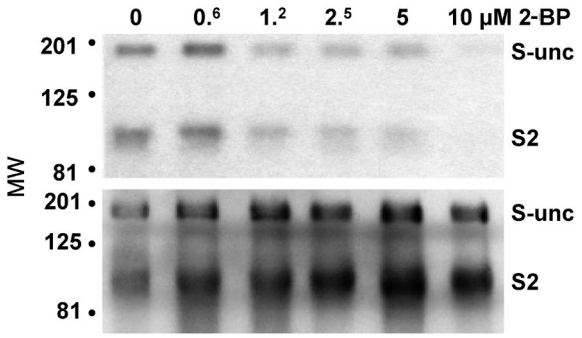

FIG. 4. Effect of 2-BP on the distribution of S proteins between cells and media. MHV (strain A59)-infected 17cl1 cells were incubated with the indicated concentrations of 2-BP from 1 to 9 hpi, and then media were collected and cells dissolved in PBS containing 0.5% NP-40. S proteins in clarified media and cell lysates were immunoprecipitated, and S proteins captured from 10^4 cell equivalents were then electrophoresed and visualized by Western immunoblotting. S-unc, uncleaved S; MW, molecular weights in thousands.

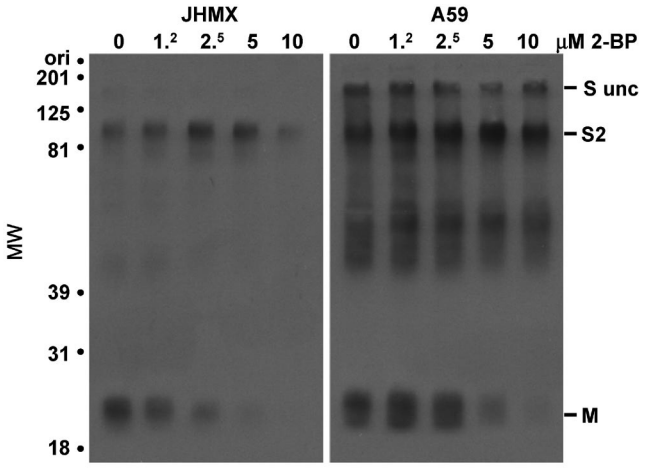

FIG. 6. Effect of 2-BP on the abundance of coimmunoprecipitating S-M complexes. 17c11 cells infected with JHMX (multiplicity of infection = 0.1) or A59 (multiplicity of infection = 1) were cultured with the indicated 2-BP doses from 1 to 9 hpi and then dissolved in NP-40/DOC buffer as described in Materials and Methods. Clarified extracts were mixed overnight with magnetic protein A–NCEA-Fc beads, which bound the S proteins. Proteins on magnet-captured beads were eluted with SDS, electrophoresed, and analyzed by immunoblotting using a cocktail of S- and M-specific MAbs. ori, origin of resolving gel; S unc, uncleaved S; MW, molecular weights in thousands.

were further addressed by inspecting electropherograms depicting ^{35}S-labeled virion proteins. From virions secreted during a 16- to 20-hpi ^{35}S-labeling period, we found that the relative proportion of S proteins did indeed decline with increasing 2-BP exposure (Fig. 5), as measured relative to virion M and N proteins. The absence of S proteins from virions was more pronounced than that observed for medium-associated S at 9 hpi (Fig. 4), and we suspect that this stems from the longer 2-BP exposures that took place prior to the virion radiolabeling process. This failure to incorporate S proteins into virions is a likely contributor to the low specific infectivity of virions secreted from 2-BP-treated cells (Fig. 2).

A possible explanation for the interference with S protein incorporation into secreted virions appeals to disruption of S protein interaction with M proteins, since S-M intracellular complexes are generally considered to be essential assembly intermediates. Thus, we infected cultures in graded doses of 2-BP, collected media, and then dissolved cell monolayers in a buffer containing both NP-40 and DOC. This detergent formulation is known to dissolve cell membranes while preserving associations between S and M proteins (28). Immunoprecipitations were then employed to capture free S and S-M complexes, which were subsequently imaged by Western immunoblotting. Indeed, the poor incorporation of S proteins into virions correlated with their failure to associate with M proteins (Fig. 6). This was most evident in cultures incubated with the higher 5 and 10 μM 2-BP doses but could be observed in JHMX-infected cells incubated with as little as 1 μM 2-BP. The 2-BP drug exposures did not exert any direct effects on the synthesis or assembly competence of the M proteins themselves, as evidenced by the abundant M (and N) proteins in secreted virions (Fig. 5). Therefore, this pharmacologic approach with 2-BP suggested that S protein palmitoylation is a prerequisite for its binding to M proteins and consequently for its effective incorporation into virions.

Effect of 2-BP on S protein palmitoylation. Given its extreme effects during MHV infection, we expected that we could measure the extent to which 2-BP might interfere with protein

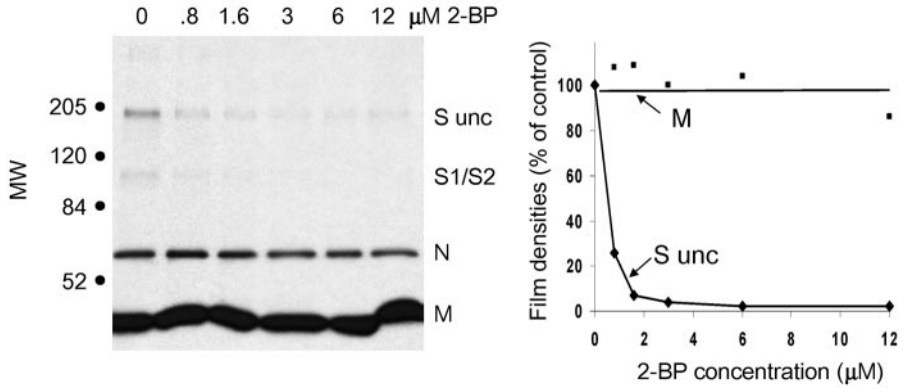

FIG. 5. Electrophoretic profiles of ^{35}S-labeled virion proteins. Virions were metabolically radiolabeled with ^{35}S amino acids and purified on density gradients as described in the legend to Fig. 2. Equal ^{35}S radioactivities were collected from each purified virion preparation, electrophoresed on SDS gels, and detected by autoradiography (left panel). Quantification of exposed film densities was obtained by densitometry, and values for S and M were plotted relative to those for control virions produced in the absence of 2-BP (right panel). MW, molecular weights in thousands.

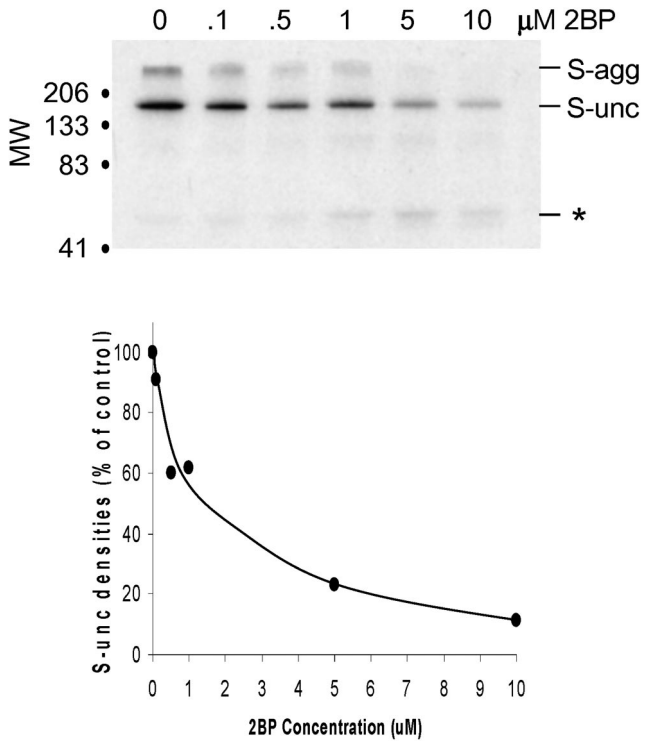

FIG. 7. Effect of 2-BP on incorporation of [^{3}H]palmitate onto S proteins. 17cl1 cells infected with A59 (multiplicity of infection = 2) were incubated from 1 to 16 hpi with the indicated 2-BP doses and then pulse labeled with [^{3}H]palmitate from 16 to 20 hpi, maintaining the indicated 2-BP concentrations throughout. Cells were dissolved in NP-40 buffer, and S proteins were immunoprecipitated from clarified lysates using magnetic protein A–NCEA-Fc beads. Radioactive S proteins were imaged by fluorography after electrophoresis on SDS-polyacrylamide gels. S-agg, aggregated S oligomers; S-unc, uncleaved S; *, S proteolytic fragments; MW, molecular weights in thousands.

palmitoylations (48). To this end, we again established infected 17cl1 cultures in graded doses of 2-BP and radiolabeled them with [^{3}H]palmitate, using the more robust strain A59 to foster detection of the weak ^{3}H label. At the peak of infection, we then lysed cells, immunoprecipitated S proteins, and visualized them on SDS gels by fluorography.

Increasing doses of 2-BP correlated with relatively nominal declines in the [^{3}H]palmitate labeling of uncleaved S proteins (Fig. 7) to levels about 10 to 15% of the control level at the 10 μM dose. This decreasing S-protein acylation was consistent with the hypothesis that ER-localized PAT activities are inhibited by 2-BP, since uncleaved S proteins are substrates for palmitoylation in the ER. In conjunction with the results of Fig. 4 to 6, these data also demonstrated that even modest declines in S-protein palmitoylation created dramatic losses in their virion incorporation. The decreasing levels of uncleaved-S palmitoylation also correlated with increasing amounts of cell-associated, ^{3}H palmitoylated proteolytic fragments of molecular weights lower than that of S2 (Fig. 7, note the bands adjacent to the asterisk), suggesting that underpalmitoylated S proteins encounter cellular proteases. The collective findings provided evidence that even modestly underpalmitoylated S proteins are faulty subunits that do not engage in virion assembly.

Effect of 2-BP on distribution of cell-associated S proteins. Our data suggested that underpalmitoylated S proteins transit to infected cell surfaces even in the presence of 10 μM 2-BP (Fig. 7) but then fail to elicit cell-cell fusions (Fig. 3E and F). To explain this significant inhibition of S-mediated syncytia occurring after exposure to relatively high doses of 2-BP, we addressed the hypothesis that S protein palmitates influence the abundance or distribution of S proteins on infected cell surfaces. Indeed, protein modification with multiple palmitates may increase partitioning into lipid rafts (1), making it reasonable to speculate that S proteins produced in the presence of high 2-BP doses might not be condensed into lipid rafts, thereby reducing their ability to cooperate in syncytial developments. This idea was first investigated by determining whether any S proteins were in fact associated with lipid rafts. DRMs are generally viewed as in vitro correlates of dynamic lipid rafts (31); therefore, we isolated these membrane fractions by floatation in sucrose gradients. Our results indicated that a small but significant proportion of cell-associated S proteins were in our DRM fractions, both in MHV-infected cells (Fig. 8A) and in cells infected with a vaccinia virus encoding MHV S proteins (Fig. 8B). In this regard, the S proteins were set apart from the VSV G proteins, which are generally used as indicators of raft exclusion (Fig. 8C) (37). Notably, low-density DRM fractions contained both uncleaved S and cleaved S2 fragments (Fig. 8B), suggesting an early, pre-trans-Golgi entrance of S proteins into lipid microdomains.

Having demonstrated that a portion of S proteins were indeed embedded in DRMs, we pursued the question of whether 2-BP redistributes membrane associations. For these experiments, we restricted analyses to S proteins on the plasma membrane, using a non-membrane-permeative protein biotinylating agent to modify exposed ectodomains prior to S immunoprecipitation and detection of the biotin tags on Western blots. Cell surface biotinylated S proteins were detected in the 2-BP-treated cultures at levels similar to those of control cultures undergoing cell-cell fusions (data not shown), indicating that the absence of syncytia in 2-BP-treated cultures (Fig. 3E and F) could not be explained by failure of S transport. Floatation of membranes in sucrose gradients revealed that the cell surface S proteins in cultures exposed to 2-BP were largely in the high-density, TX100-soluble material, unlike control S proteins, where ~30% were DRM associated (Fig. 8D to F). Therefore, we suggest that S-protein palmitoylations are necessary to condense free S proteins into lipid raft microdomains, where they cooperate to mediate syncytia. This lipid raft partitioning would have considerable biological relevance for those coronaviruses exhibiting pH-independent S-mediated fusion activities, since this would allow infections to spread via cell-cell fusions.

Molecular genetic evidence for the contribution of palmitoylated cysteines to virus infectivity. Using the pharmacologic approach involving 2-BP, we obtained evidence that palmitoylations were necessary for assembly of S proteins into virions. To determine whether all of the acylated thiols are involved in these assembly reactions or whether some are alternatively necessary only for postassembly functions, we employed a complementary molecular genetic approach in which individual cysteine substrate sites were mutated. This was not a trivial undertaking, because the number of potentially palmitoylated

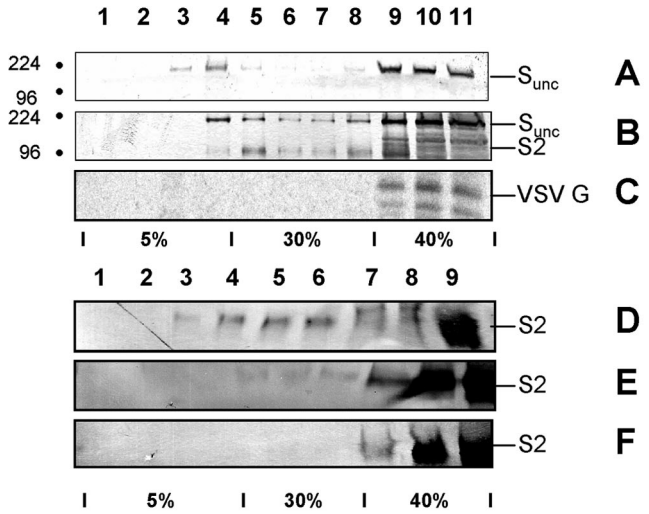

FIG. 8. S-protein association with detergent-resistant membranes and effect of 2-BP on distribution of S proteins in the plasma membrane. (A-C) HeLa-CEACAM cells were infected with MHV strain JHMX (A), vaccinia recombinants vTF7.3 and vTM1-S-JHMX (14), or VSV (C). At 8 hpi, infected cultures were dissolved in cold Triton X-100 and lysates subjected to flotation in sucrose density gradients, as described in Materials and Methods. Gradients were fractionated from air-gradient interfaces, and proteins were recognized by Western immunoblotting using S- and VSV G-specific antibodies. (D-F) 17cl1 cells were infected with MHV strain JHMX, and at 1 hpi, 0 μM (D), 10 μM (E), or 25 μM (F) 2-BP doses were added. At 16 hpi, sulfo-NHS-LC-biotin was briefly applied and the unreacted reagent quenched with glycine. Cells were then dissolved in cold Triton X-100 buffer and lysates centrifuged to equilibrium in sucrose density gradients. S proteins in the gradient fractions were immunoprecipitated, and the biotinylated subpopulations were recognized on Western blots using streptavidin-horseradish peroxidase conjugate and a colorimetric assay for the immobilized horseradish peroxidase. S_{unc}, uncleaved S.

cysteines at the boundary between S protein transmembrane and cytoplasmic domains is very large (Fig. 9A) and the amino acid chosen to replace each cysteine can generate unexpected outcomes. Additionally, the profoundly disabling effects of 2-BP made it likely that most if not all cysteine mutants would compromise infectivities, perhaps to an extent precluding their isolation. We did, however, have the advantage of earlier results by Bos et al. (2) and Chang et al. (7) revealing some residual S-protein syncytial activities after mutation of two acylatable cysteines in the middle of the cysteine-rich region (indicated by the asterisks in Fig. 9A). Thus, we could infer that such mutant S proteins would provide the receptor-binding and membrane fusion functions required for virus viability, making it possible to ask whether the mutations were compatible with S assembly into virions.

We constructed mutant cDNAs encoding the 3′-terminal 9,330 nucleotides of MHV (JHM) and created in vitro JHM transcripts for targeted RNA recombination. Recombinant JHM viruses were then generated in feline cells simultaneously infected with feline MHV-JHM (21, 27) and transfected with the in vitro JHM transcripts. Selection of the rare recombinant JHM (rJHM) mutants was achieved by plaque isolation on murine 17cl1 cells. This powerful reverse genetics technique, developed by the Masters and Rottier laboratories (23), allowed us to plaque isolate two rJHM viruses with cysteine substitutions. Successful isolation of these mutant viruses was fostered by our choice of JHM as the parent strain, since JHM is so highly syncytial on 17cl1 cells that even severely debilitated mutants can often be recognized. Indeed, the mutant viruses, rJHM-C1348F and rJHM-C1347F/C1348S, demonstrated slow growth kinetics relative to those of parental rJHM (Fig. 9B) but could nonetheless be passaged several times without reversion. This slow growth could be attributed to delayed expansion of the mutant virus infections through tissue cultures (Fig. 9C), a predictable result in light of previous observations on the importance of the cysteine-rich region in S-mediated fusion activities.

Virions were purified from the infected cultures to assess relative S-protein content and specific infectivity. We found that the C1348S mutant particles were similar to parental rJHM in both virion protein content and infectivity (data not shown). However, we were surprised to find that virions derived from the most impaired C1347F/C1348S infections were not deficient in S proteins; in fact, they were slightly more replete with S than the corresponding parental rJHM (Fig. 9D). Thus, it appears that S-protein incorporation into virions does not require that the cysteine-rich region be saturated with hydrophobic acylations—at least cysteine substrates 1347 and 1348 are dispensable in assembly. The cysteines did contribute more subtly to the final assembled virion structure, since S proteins with substitutions at 1347 and 1348 were distinguished in the electropherograms by a small proportion of ~180-kDa uncleaved S and by an increased proportion of SDS-solubilized ~90-kDa S2 fragments (Fig. 9D). These unique protein biochemical properties correlated with reduced specific infectivities. Two independent determinations revealed infectivities for the C1347S/C1348F mutants that were 10-fold lower than the unaltered parental recombinants (Fig. 9D). The properties of these virions with cysteine substitutions made it clear that either the thiols themselves or their attached acyl chains are intrinsic contributors to virion architecture and infectivity.

DISCUSSION

All coronaviruses encode S proteins with cysteine-rich cytoplasmic tails (6). The essential nature of the cysteine-rich region is suggested by its strict conservation and by the fact that more than one of the thiols are substrates for posttranslational palmitoylation (2). Important molecular genetic analyses have indeed pointed toward the essential roles for the cysteine-rich region in S functions (3, 54), specifically in mediating membrane fusion (2, 7). In this study, we used a pharmacologic approach to discover roles for the posttranslational palmitoylation of the cytoplasmic cysteines of the coronavirus proteins. Using 2-BP to interfere with cellular PAT activities, we established correlations between murine coronavirus S protein acylation, S-protein–M-protein interaction, and infective virion assembly. Therefore, we suggest that it is not the cysteines per se that are relevant to assembly, but it is rather that they act as substrates for palmitoylation and that one or more of the hydrophobic acyl chains are essential components of assembly-competent S proteins. Coronavirus assembly and budding occurs in the ER or *cis*-Golgi complex (19); therefore, we further suggest that ER or *cis*-Golgi-localized PAT activities are essential components of the coronavirus-permissive cell.

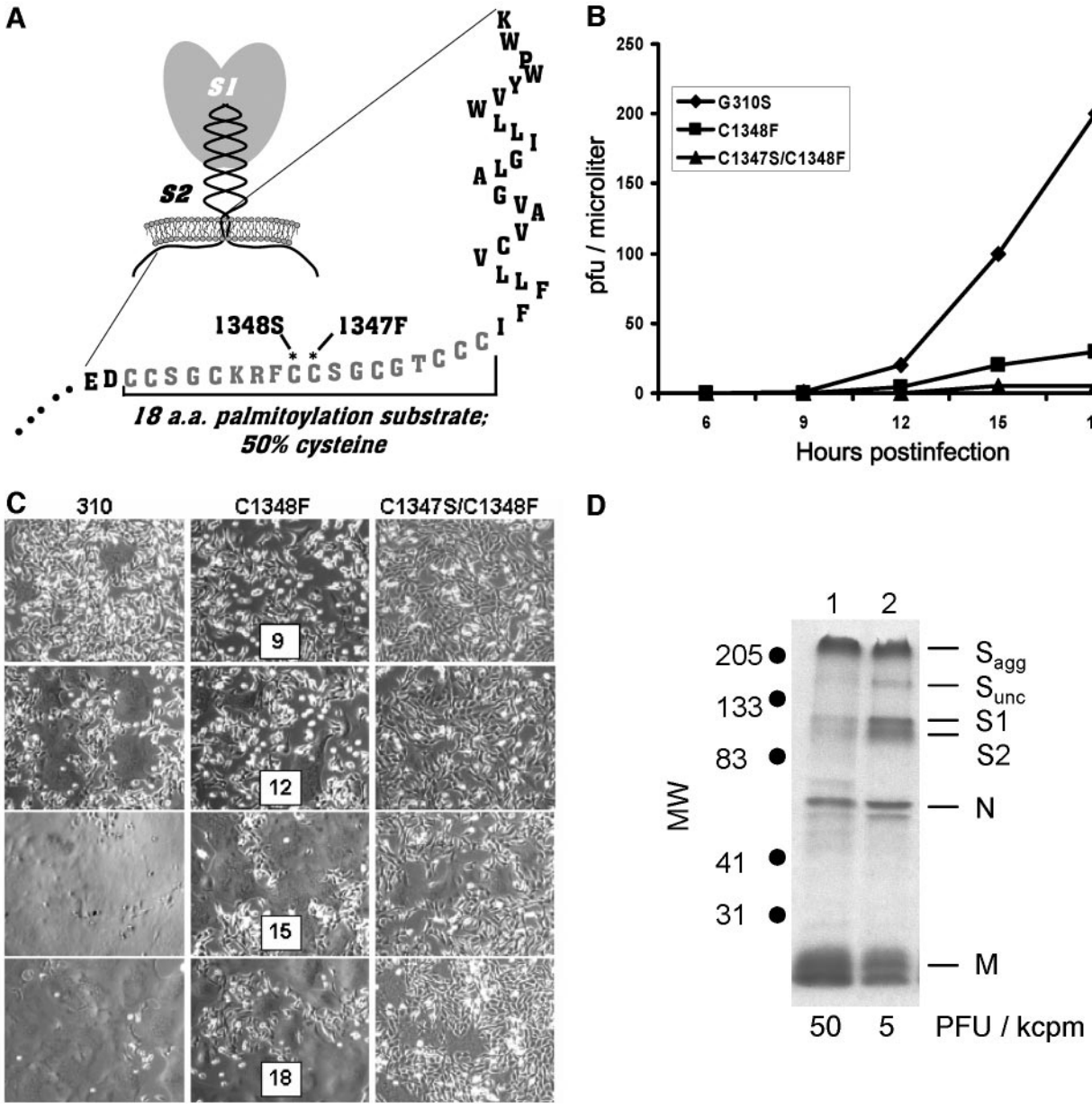

FIG. 9. Isolation and characterization of C1347F and C1347F/C1348S MHV mutants. (A) A S-protein trimer is depicted with transmembrane span and cysteine-rich residues illustrated in the context of the virion membrane. Mutations chosen for introduction into recombinant viruses are indicated by the asterisks. (B) Growth kinetics of wild-type JHM-G310S (26), -C1347F, and -C1347F/C1348S. 17c11 cells were infected with recombinant JHM isolates at 0.01 PFU/cell. Output titers were determined in culture supernatants collected at the indicated hours postinfection, using HeLa-CEACAM cells as plaque indicators. (C) Syncytial expansion of JHM-G310S, -C1347F, and -C1347F/C1348S infections. HeLa-CEACAM cells were infected with JHM isolates at 0.01 PFU/cell, and photographs were taken at the indicated hours postinfection (numbers in center panels). (D) Electrophoretic profiles of rJHM-G310S (lane 1) and rJHM-G310S with the C1347F and C1348S mutations (lane 2). Infected 17cl1 cells were radiolabeled with ^{35}S amino acids from 20 to 28 hpi, media were collected, and virions were purified by two cycles of equilibrium sucrose density gradient centrifugation. Virion proteins were electrophoresed on SDS gels and visualized by fluorography. Specific infectivities of the virion preparations (PFU/^{35}S cpm) are indicated beneath each lane. MW, molecular weights in thousands.

Our investigations uncovered interesting effects of 2-BP on MHV infection parameters. In MHV-infected 17cl1 fibroblast cells, extraordinarily low 2-BP doses had significant inhibitory effects on infective virion secretion but actually enhanced S-mediated intercellular fusions. This condition was met when total S-protein palmitoylation levels were reduced by ~40%. Thus, when PAT activities are only modestly reduced, the infection shifts from a productive one in which virions are secreted to an overtly cytopathic, syncytial condition that sheds noninfectious virus particles. From these results, we suggest that one or more of the fatty acids on S proteins are more crucial to the virus assembly process than they are to S-induced syncytial developments. This suggestion assumes that 2-BP indiscriminately inhibits PAT activities at sites in the exocytic pathway that are both proximal and distal to the virus budding site. Indeed, it remains possible that 2-BP preferentially blocks

ER-localized PATs, thus accounting for its antivirion specificity at low doses. If this were the case, we would favor a slightly different view in which coronavirus infection patterns depend on the subcellular distribution of PAT activities. Abundant ER/*cis*-Golgi-localized PAT would correlate with efficient infective virion assembly and secretion, while distally located Golgi/plasma membrane PATs could only assist in creating syncytial developments. A corollary suggestion is that ER-localized PAT activities regulate the segregation of S proteins between assembling virions and infected-cell surfaces.

Exposure of MHV-infected 17cl1 cells to higher doses of 2-BP abrogated S-mediated syncytial activities. 2-BP did not arrest S transport to cell surfaces; in fact, the opposite occurred as the underpalmitoylated S proteins were not trapped intracellularly in association with M. However, the underpalmitoylated S proteins were partitioned out of DRMs. From these findings, we suggest a secondary role for S-protein palmitoylations, namely, to enhance affinity for lipid raft localization on cell surfaces. We contend that this is a secondary function of acyl groups that is independent of their role during virion assembly. Multiple closely spaced acylations are well-known structures providing for lipid raft partitioning (25, 33). Similarly, we expected that S redistribution out of raft locations would correlate with diminished syncytia. Viral glycoprotein clustering is generally considered to be a prerequisite for the cooperative process by which membrane fusion pores are created (8, 43). Therefore, we are presently favoring a view in which palmitoylations act to cluster S proteins on plasma membranes enough for their cooperative action in fusing opposing membranes. However, our data do not distinguish whether the loss of syncytial activity is intrinsic to underpalmitoylated S proteins or is merely secondary to their dispersion on cell surfaces.

On membrane proteins, two thiols are known to be sufficient for multiple acylation and subsequent lipid raft partitioning (33), but the cytoplasmic tails of coronavirus S proteins, without exception, have 7 to 10 cysteines (6) (Fig. 9A). Thus, the cysteine-rich regions on S proteins appear to have expanded beyond the level necessary for lipid raft partitioning and fusion activity at infected-cell surfaces. We suggest that the expansive cysteine-rich regions have evolved in response to cellular limitations for ER-localized PAT activities. A display of dense cysteine clusters is perhaps the only way to insure that a sufficient portion of newly synthesized S proteins are palmitoylated enough to serve as proper virion assembly subunits. In support of this view, we note that virion assembly competence is universally required but syncytial competence is not. For example, severe acute respiratory syndrome-associated coronavirus infections are not normally syncytial because the S proteins are fusion active at pH values below those found in extracellular fluids (38). Evolutionary selection for cell surface S protein clustering into fusion-active arrangements is therefore unlikely.

2-BP exposures reduced the levels of S proteins in secreted virions, but the cysteine substitution mutations C1347F and C1348S did not. Notably, eliminating these two thiols does not prevent all S acylation (2), and so we suggest that a subset of the S cytoplasmic cysteines serve as the crucial preassembly acylation substrates—cysteines 1347 and 1348 are clearly not included in this subset. We believe that the essential subset minimally includes C1344, since we were never successful at fixing amino acid substitutions at this position into viable recombinant MHVs (data not shown). More extensively mutagenized constructs with substitution of all nine cysteines in the palmitoylation substrate (Fig. 9A) were similarly incompatible with viability. We note that a definitive identification of the acylation substrates required for assembly will have to await results of assays for mutant S-protein incorporation into coronavirus-like particles (3, 11), since we cannot base firm conclusions solely on the basis of negative outcomes from recombinant virus preparation.

While cysteines 1347 and 1348 are dispensable in assembly, they are nonetheless key contributors of native virion structure and robust virus particle infectivity. On the basis of earlier findings by Bos et al. (2), we believe that one or both of these cysteines are palmitoylation substrates, and so we suggest that these S acylations specifically contribute to infectivity at steps distinct from virus assembly. How might these multiple acylations contribute to particle infectivities? An interesting speculation is that the abundant acyl chains linked to the three cytoplasmic tails of each S2 trimer assist in creating lipid bilayer "rings," insuring relatively high lipid content around S proteins. Such lipid surroundings may be necessary for virion entry. During the enveloped-virus entry process, there is a concerted refolding of the surface glycoproteins mediating membrane fusion (17). While the details of the refolding process are not yet known for coronavirus S proteins, the reaction fits the model for "class 1" viral fusion proteins (4). In this model, hydrophobic peptides move from the interior of the proteins and insert in cellular membranes, and then the proteins refold into end-stage structures, bringing the cell membrane-intercalated peptides toward the virion membrane to create the proximities necessary for cell-virion membrane fusion. This refolding process demands that there be no impediments to juxtaposing hydrophobic S fusion peptides with S transmembrane spans. Coronavirus assembly involves S-protein–M-protein interactions (11), while coronavirus entry demands that the M proteins not obstruct S-protein refolding. Our current view is that some S acylations create assembly competence, while other, additional S acylations might maintain other proteins, notably M, at an appropriate distance so that S protein refolding and membrane fusion reactions can be successfully completed.

ACKNOWLEDGMENTS

We thank Fumihiro Taguchi (National Institute of Neuroscience, Tokyo, Japan) and John Fleming (University of Wisconsin) for anti-S and anti-M antibodies. We thank Paul Masters (Wadsworth Center, New York State Department of Health) and Stanley Perlman (University of Iowa) for the plasmid vectors used to create recombinant mutant MHVs. We also thank Chandra Tangudu, Heidi Olivares, and Stanley Perlman for their comments during the preparation of the manuscript.

This work was supported by NIH grant 60030.

REFERENCES

1. **Arni, S., S. A. Keilbaugh, A. G. Ostermeyer, and D. A. Brown.** 1998. Association of GAP-43 with detergent-resistant membranes requires two palmitoylated cysteine residues. J. Biol. Chem. **273:**28478–28485.
2. **Bos, E. C. W., L. Heijnen, W. Luytjes, and W. J. M. Spaan.** 1995. Mutational analysis of the murine coronavirus spike protein: effect on cell-to-cell fusion. Virology **214:**453–463.
3. **Bosch, B. J., C. A. de Haan, S. L. Smits, and P. J. Rottier.** 2005. Spike protein assembly into the coronavirion: exploring the limits of its sequence requirements. Virology **334:**306–318.

4. **Bosch, B. J., R. van der Zee, C. A. de Haan, and P. J. Rottier.** 2003. The coronavirus spike protein is a class I virus fusion protein: structural and functional characterization of the fusion core complex. J. Virol. **77:**8801–8811.
5. **Brown, D.** 2002. Structure and function of membrane rafts. Int. J. Med. Microbiol. **291:**433–437.
6. **Cavanagh, D.** 1995. The coronavirus surface glycoprotein, p. 73–115. *In* S. G. Siddell, ed., The Coronaviridae. Plenum Press, New York, N.Y.
7. **Chang, K. W., Y. Sheng, and J. L. Gombold.** 2000. Coronavirus-induced membrane fusion requires the cysteine-rich domain in the spike protein. Virology **269:**212–224.
8. **Danieli, T., S. L. Pelletier, Y. I. Henis, and J. M. White.** 1996. Membrane fusion mediated by the influenza virus hemagglutinin requires the concerted action of at least three hemagglutinin trimers. J. Cell Biol. **133:**559–569.
9. **Davies, H. A., and M. R. Macnaughton.** 1979. Comparison of the morphology of three coronaviruses. Arch. Virol. **59:**25–33.
10. **de Haan, C. A., K. Stadler, G. J. Godeke, B. J. Bosch, and P. J. Rottier.** 2004. Cleavage inhibition of the murine coronavirus spike protein by a furin-like enzyme affects cell-cell but not virus-cell fusion. J. Virol. **78:**6048–6054.
11. **de Haan, C. A. M., M. Smeets, F. Vernooij, H. Vennema, and P. J. M. Rottier.** 1999. Mapping of the coronavirus membrane protein domains involved in interaction with the spike protein. J. Virol. **73:**7441–7452.
12. **Dunphy, J. T., W. K. Greentree, C. L. Manahan, and M. E. Linder.** 1996. G-protein palmitoyltransferase activity is enriched in plasma membranes. J. Biol. Chem. **271:**7154–7159.
13. **Fuerst, T. R., P. L. Earl, and B. Moss.** 1987. Use of a hybrid vaccinia virus-T7 RNA polymerase system for expression of target genes. Mol. Cell. Biol. **7:**2538–2544.
14. **Gallagher, T. M.** 1997. A role for naturally occurring variation of the murine coronavirus spike protein in stabilizing association with the cellular receptor. J. Virol. **71:**3129–3137.
15. **Gossen, M., and H. Bujard.** 1992. Tight control of gene expression in mammalian cells by tetracycline-responsive promoters. Proc. Natl. Acad. Sci. USA **89:**5547–5551.
16. **Harder, T., P. Scheiffele, P. Verkade, and K. Simons.** 1998. Lipid domain structure of the plasma membrane revealed by patching of membrane components. J. Cell Biol. **141:**929–942.
17. **Jardetzky, T. S., and R. A. Lamb.** 2004. Virology: a class act. Nature **427:**307–308.
18. **Jin, H., K. Subbarao, S. Bagai, G. P. Leser, B. R. Murphy, and R. A. Lamb.** 1996. Palmitylation of the influenza virus hemagglutinin (H3) is not essential for virus assembly or infectivity. J. Virol. **70:**1406–1414.
19. **Krijnske-Locker, J., M. Ericsson, P. J. Rottier, and G. Griffiths.** 1994. Characterization of the budding compartment of mouse hepatitis virus: evidence that transport from the RER to the Golgi complex requires only one vesicular transport step. J. Cell Biol. **124:**55–70.
20. **Krueger, D. K., S. M. Kelly, D. N. Lewicki, R. Ruffolo, and T. M. Gallagher.** 2001. Variations in disparate regions of the murine coronavirus spike protein impact the initiation of membrane fusion. J. Virol. **75:**2792–2802.
21. **Kuo, L., G. J. Godeke, M. J. Raamsman, P. S. Masters, and P. J. Rottier.** 2000. Retargeting of coronavirus by substitution of the spike glycoprotein ectodomain: crossing the host cell species barrier. J. Virol. **74:**1396–1406.
22. **Makino, S., F. Taguchi, and K. Fujiwara.** 1984. Defective interfering particles of mouse hepatitis virus. Virology **133:**9–17.
23. **Masters, P. S., and P. J. Rottier.** 2005. Coronavirus reverse genetics by targeted RNA recombination. Curr. Top. Microbiol. Immunol. **287:**133–159.
24. **McLaughlin, R. E., and J. B. Denny.** 1999. Palmitoylation of GAP-43 by the ER-Golgi intermediate compartment and Golgi apparatus. Biochim. Biophys. Acta **1451:**82–92.
25. **Melkonian, K. A., A. G. Ostermeyer, J. Z. Chen, M. G. Roth, and D. A. Brown.** 1999. Role of lipid modifications in targeting proteins to detergent-resistant membrane rafts: many raft proteins are acylated, while few are prenylated. J. Biol. Chem. **274:**3910–3917.
26. **Ontiveros, E., T. S. Kim, T. M. Gallagher, and S. Perlman.** 2003. Enhanced virulence mediated by the murine coronavirus, mouse hepatitis virus strain JHM, is associated with a glycine at residue 310 of the spike glycoprotein. J. Virol. **77:**10260–10269.
27. **Ontiveros, E., L. Kuo, P. S. Masters, and S. Perlman.** 2001. Inactivation of expression of gene 4 of mouse hepatitis virus strain JHM does not affect virulence in the murine CNS. Virology **289:**230–238.
28. **Opstelten, D.-J. E., M. J. B. Raamsman, K. Wolfs, M. C. Horzinek, and P. J. M. Rottier.** 1995. Envelope glycoprotein interactions in coronavirus assembly. J. Cell Biol. **131:**339–349.
29. **Perlman, S.** 1998. Pathogenesis of coronavirus-induced infections. Adv. Exp. Med. Biol. **440:**503–513.
30. **Phillips, J. J., M. M. Chua, E. Lavi, and S. R. Weiss.** 1999. Pathogenesis of chimeric MHV4/MHVA59 recombinant viruses: the murine coronavirus spike protein is a major determinant of neurovirulence. J. Virol. **73:**7752–7760.
31. **Pralle, A., P. Keller, E. L. Florin, K. Simons, and J. K. Horber.** 2000. Sphingolipid-cholesterol rafts diffuse as small entities in the plasma membrane of mammalian cells. J. Cell Biol. **148:**997–1008.
32. **Rao, P. V., and T. M. Gallagher.** 1998. Intracellular complexes of viral spike and cellular receptor accumulate during cytopathic murine coronavirus infections. J. Virol. **72:**3278–3288.
33. **Resh, M. D.** 2004. Membrane targeting of lipid modified signal transduction proteins. Subcell. Biochem. **37:**217–232.
34. **Rocks, O., A. Peyker, M. Kahms, P. J. Verveer, C. Koerner, M. Lumbierres, J. Kuhlmann, H. Waldmann, A. Wittinghofer, and P. I. Bastiaens.** 2005. An acylation cycle regulates localization and activity of palmitoylated Ras isoforms. Science **307:**1746–1752.
35. **Rousso, I., M. B. Mixon, B. K. Chen, and P. S. Kim.** 2000. Palmitoylation of the HIV-1 envelope glycoprotein is critical for viral infectivity. Proc. Natl. Acad. Sci. USA **97:**13523–13525.
36. **Sawicki, S. G.** 1987. Characterization of a small plaque mutant of the A59 strain of mouse hepatitis virus defective in cell fusion. Adv. Exp. Med. Biol. **218:**169–174.
37. **Scheiffele, P., A. Rietveld, T. Wilk, and K. Simons.** 1999. Influenza viruses select ordered lipid domains during budding from the plasma membrane. J. Biol. Chem. **274:**2038–2044.
38. **Simmons, G., J. D. Reeves, A. J. Rennekamp, S. M. Amberg, A. J. Piefer, and P. Bates.** 2004. Characterization of severe acute respiratory syndrome-associated coronavirus (SARS-CoV) spike glycoprotein-mediated viral entry. Proc. Natl. Acad. Sci. USA **101:**4240–4245.
39. **Smit, J. M., R. Bittman, and J. Wilschut.** 2001. Deacylation of the transmembrane domains of Sindbis virus envelope glycoproteins E1 and E2 does not affect low-pH-induced viral membrane fusion activity. FEBS Lett. **498:**57–61.
40. **Smotrys, J. E., and M. E. Linder.** 2004. Palmitoylation of intracellular signaling proteins: regulation and function. Annu. Rev. Biochem. **73:**559–587.
41. **Sturman, L. S., C. S. Ricard, and K. V. Holmes.** 1985. Proteolytic cleavage of the E2 glycoprotein of murine coronavirus: activation of cell-fusing activity of virions by trypsin and separation of two different 90K cleavage fragments. J. Virol. **56:**904–911.
42. **Sturman, L. S., and K. K. Takemoto.** 1972. Enhanced growth of a murine coronavirus in transformed mouse cells. Infect. Immun. **6:**501–507.
43. **Takeda, M., G. P. Leser, C. J. Russell, and R. A. Lamb.** 2003. Influenza virus hemagglutinin concentrates in lipid raft microdomains for efficient viral fusion. Proc. Natl. Acad. Sci. USA **100:**14610–14617.
44. **Thorp, E. B., and T. M. Gallagher.** 2004. Requirements for CEACAMs and cholesterol during murine coronavirus cell entry. J. Virol. **78:**2682–2692.
45. **Tooze, J., S. Tooze, and G. Warren.** 1984. Replication of coronavirus MHV-A59 in sac− cells: determination of the first site of budding of progeny virions. Eur. J. Cell Biol. **33:**281–293.
46. **van Berlo, M. F., W. J. van den Brink, M. C. Horzinek, and B. A. M. van der Zeijst.** 1987. Fatty acid acylation of viral proteins in murine hepatitis virus-infected cells. Arch. Virol. **95:**123–130.
47. **Varner, A. S., M. L. De Vos, S. P. Creaser, B. R. Peterson, and C. D. Smith.** 2002. A fluorescence-based high performance liquid chromatographic method for the characterization of palmitoyl acyl transferase activity. Anal. Biochem. **308:**160–167.
48. **Veit, M., L. E. Dietrich, and C. Ungermann.** 2003. Biochemical characterization of the vacuolar palmitoyl acyltransferase. FEBS Lett. **540:**101–105.
49. **Vennema, H., G. J. Godeke, J. W. Rossen, W. F. Voorhout, M. C. Horzinek, D. J. Opstelten, and P. J. Rottier.** 1996. Nucleocapsid-independent assembly of coronavirus-like particles by co-expression of viral envelope protein genes. EMBO J. **15:**2020–2028.
50. **Wagner, R., A. Herwig, N. Azzouz, and H. D. Klenk.** 2005. Acylation-mediated membrane anchoring of avian influenza virus hemagglutinin is essential for fusion pore formation and virus infectivity. J. Virol. **79:**6449–6458.
51. **Webb, Y., L. Hermida-Matsumoto, and M. D. Resh.** 2000. Inhibition of protein palmitoylation, raft localization, and T cell signaling by 2-bromopalmitate and polyunsaturated fatty acids. J. Biol. Chem. **275:**261–270.
52. **Weiner, L. P.** 1973. Pathogenesis of demyelination induced by a mouse hepatitis virus (JHM virus). Arch. Neurol. **28:**298–303.
53. **Whitt, M. A., and J. K. Rose.** 1991. Fatty acid acylation is not required for membrane fusion activity or glycoprotein assembly into VSV virions. Virology **185:**875–878.
54. **Ye, R., C. Montalto-Morrison, and P. S. Masters.** 2004. Genetic analysis of determinants for spike glycoprotein assembly into murine coronavirus virions: distinct roles for charge-rich and cysteine-rich regions of the endodomain. J. Virol. **78:**9904–9917.
55. **Zhang, S. X., Y. Han, and G. W. Blissard.** 2003. Palmitoylation of the *Autographa californica* multicapsid nucleopolyhedrovirus envelope glycoprotein GP64: mapping, functional studies, and lipid rafts. J. Virol. **77:**6265–6273.
56. **Zurcher, T., G. Luo, and P. Palese.** 1994. Mutations at palmitylation sites of the influenza virus hemagglutinin affect virus formation. J. Virol. **68:**5748–5754.